Journal of Computational Mathematics, Vol.19, No.6, 2001, 617–628.

COMPUTATION OF NONEQUILIBRIUM HYPERSONIC FLOW OVER CONCAVE CORNERS*[1)]

Taehoon Park
(*Department of Mathematics, Kookmin University, Seoul 136-702, Korea*)

You-lan Zhu
(*Department of Mathematics, The University of North Carolina at Charlotte, USA*)

Abstract

This paper is devoted to computation of hypersonic flow of air with chemical reactions over concave corners. A technique combining smooth transformation of domain and implicit difference methods is used to overcome numerical difficulties associated with the lack of resolution behind the shock and near the body. The implicit treatment of right hand side terms is also an important part of our method.

Key words: Shock fitting, Smooth transformation of domain, Finite difference method, Implicit method.

1. Introduction

We consider steady inviscid hypersonic flow of air about a concave corner including chemical reaction effects. Computation of nonequilibrium flow is difficult because of the steep gradients behind the shock and an entropy layer near the body. For many cases the time scale of the chemical reactions is larger than, or close to, the time scale of the original mechanical problem and the equilibrium chemistry model is not realistic. Therefore, it is necessary to evaluate the kinetics of chemistry via a nonequilibrium model.

In 1975, Rakich *et al.* [7] applied a method of characteristics to solve supersonic inviscid nonequilibrium flows. The 5-species, 18-reaction chemical model they described has since been adopted by many others [1, 2, 4]. Later, Rakich *et al.* [8] computed the flow over a concave corner. Although their method is accurate globally, it is less accurate locally. They found that the calculation for the shock angle failed to converge, resulting in a complete loss of accuracy. They were able to compute only for a short distance because of the lack of resolution near the shock. They also found that the source term resulting from chemical reactions had a strong effect on the shock solution. In 1991, Pandolfi *et al.* [4] computed the same flow introducing generalized nonequilibrium Rankine-Hugoniot (R-H) relations at the shock instead of classical R-H conditions. Using their technique, they were able to continue the computation to a very large distance. In their result details occurring over a short distance behind the shock are not given and such details are absorbed in the generalized R-H conditions.

Our goal in this paper is to design a finite difference method that will give details of the flow near the shock and compute flow accurately for a long distance. Once this is successful, we will be able to compute more difficult problems with stronger stiffness or steeper gradients for any desirable distance. We will do this using a smooth coordinate transformation under which a mesh size near boundaries represents a small physical distance while in the middle of

* Received May 19, 1998; Final revised July 15, 2000.
[1)] This work was partially supported by the North Carolina Supercomputing Center.

the computational region it represents a large physical distance. When the mesh size in the physical domain in one direction is very small and explicit schemes are used, the mesh size in other direction must be small too. In order to make the computation efficient, we have used an implicit scheme for this problem. In this way, the computations can be done efficiently with a relatively small number of mesh points and yet the difficulty arising from lack of resolution near the shock is overcome.

2. System of Equations

The problem we consider is hypersonic flow around bodies with chemical reactions. In our chemical model of air only dissociation-recombination reactions, atom exchange reactions, and bimolecular reactions are considered. Ionization is neglected. Also the vibrational excitation of biatomic molecules is assumed half-excited so that its energy content is $RT/2$ [3]. The Euler and chemical equations are strongly coupled. We begin with the Euler equations for the steady-state configuration [4]:

$$\boldsymbol{V} \cdot \nabla \rho + \rho \nabla \cdot \boldsymbol{V} = 0, \tag{1}$$

$$(\boldsymbol{V} \cdot \nabla)\, \boldsymbol{V} + \frac{\nabla p}{\rho} = 0, \tag{2}$$

$$\boldsymbol{V} \cdot \left(\nabla h - \frac{\nabla p}{\rho} \right) = 0. \tag{3}$$

Here, $\boldsymbol{V}$, ρ, p and h denote the velocity vector, density, pressure and enthalpy respectively. We neglect the diffusion of the species and the equations of the production of the species along streamlines are as follows:

$$\boldsymbol{V} \cdot \nabla q_i = \omega_i, \quad i = 1, 2, 3. \tag{4}$$

Here, q_i denotes the concentration in unit $g\text{-}mole \cdot g^{-1}$ and the source term ω_i gives the rate of production for the i-th species.

With the same assumptions as in [4], we will describe the equations for a two dimensional computational frame $\{\eta, \xi\}$. We introduce a $\{z, r\}$-Descartes coordinate system and let

$$\sigma = \frac{v}{u} \quad \text{and} \quad V = \sqrt{u^2 + v^2}, \tag{5}$$

where u and v are components of velocity in z and r directions respectively. Taking p, h, σ, q_1, q_2, q_3 as dependent variables, we can have the following form of the Euler and the chemical equations under the $\{z, r\}$-Descartes coordinate system :

$$\left(1 - \frac{a^2}{u^2}\right) p_z + \sigma p_r + \rho a^2 \sigma_r = \frac{a^2}{u} \Psi, \tag{6}$$

$$\sigma_z + \sigma \sigma_r + \frac{p_r - \sigma p_z}{\rho u^2} = 0, \tag{7}$$

$$h_z - \frac{p_z}{\rho} + \sigma \left(h_r - \frac{p_r}{\rho} \right) = 0, \tag{8}$$

$$(q_i)_z + \sigma (q_i)_r = \frac{\omega_i}{u}, \quad i = 1, 2, 3. \tag{9}$$

The system is completed by the integrated form of the energy equation

$$H = h + \frac{V^2}{2} = \text{constant}. \tag{10}$$

Explicit formulas for h, a and Ψ can be found in [4] and related constants are given in [8].

The region confined by $r = b(\eta)$, $r = c(\eta)$, $\eta = \eta_0^*$ and $\eta = \eta_1^*$ is the physical domain for computation. The curve $r = b(\eta)$ is the body and $r = c(\eta)$ is the shock. We now introduce a computational frame (η, ξ)

$$\begin{aligned} z &= \eta \quad (\eta_0^* \le \eta \le \eta_1^*), \\ r &= G(\eta, \xi). \end{aligned}$$

Here $G(\eta, \xi)$ satisfies the conditions $b(\eta) = G(\eta, 0)$ and $c(\eta) = G(\eta, 1)$ so that $\xi = 0$ at the body and $\xi = 1$ at the shock and the computational domain under the (η, ξ)-coordinate system is a rectangle.

By using the relations

$$\begin{aligned} \frac{\partial}{\partial z} &= \xi_z \frac{\partial}{\partial \xi} + \frac{\partial}{\partial \eta}, \\ \frac{\partial}{\partial r} &= \xi_r \frac{\partial}{\partial \xi}, \end{aligned} \tag{11}$$

the derivatives with respect to z and r in (6)-(9) can be changed into the derivatives with respect to η and ξ and we obtain the corresponding system of equations under the (η, ξ)-coordinate system. The system consists of 6 equations of the form:

$$\boldsymbol{A}^* \frac{\partial \boldsymbol{U}}{\partial \eta} + \boldsymbol{B}^* \frac{\partial \boldsymbol{U}}{\partial \xi} = f, \tag{12}$$

where $\boldsymbol{A}$, $\boldsymbol{B}$ are vectors with 6 components and $\boldsymbol{U} = (p, h, \sigma, q_1, q_2, q_3)^*$ is a vector with 6 components, the superscript * indicating the transpose of the vector and f is a scalar function.

3. Numerical Procedures

If the component u of velocity is supersonic everywhere, then any line z =constant, i.e., η =constant is space-like. In this case, if initial conditions are given at $\eta = \eta_0^*$ and appropriate boundary conditions are specified at $\xi = 0$ (the body) and at $\xi = 1$ (the shock), then the initial-boundary-value problem is well-posed and the space-marching technique can be used in order to get the solution of the system on the domain: $\eta_0^* < \eta \le \eta_1^*$, $0 \le \xi \le 1$.

At the body, we have a natural boundary condition

$$\boldsymbol{V} \cdot \boldsymbol{n} = 0, \tag{13}$$

$\boldsymbol{n}$ being the unit normal vector to the body.

Since the rate of chemical reaction is finite, the shock conditions are similar to those for perfect gas flow. The quantities of flow parameters should satisfy the R-H (Rankine-Hugoniot) conditions

$$\begin{aligned} \rho_2 V_{n,2} &= \rho_1 V_{n,1}, \\ p_2 + \rho_2 V_{n,2}^2 &= p_1 + \rho_1 V_{n,1}^2, \\ h_2 + \frac{V_{n,2}^2}{2} &= h_1 + \frac{V_{n,1}^2}{2} \end{aligned} \tag{14}$$

and

$$q_{i,1} = q_{i,2}, \quad i = 1, 2, 3, \tag{15}$$

where $\boldsymbol{n}$ is the unit normal vector to the shock and $V_n = \boldsymbol{V} \cdot \boldsymbol{n}$. The quantities with index 1 mean the quantities in front of the shock and with index 2 mean those behind the shock. In this case the enthalpy h can be expressed as

$$h = \frac{\gamma p}{(\gamma - 1)\rho}. \tag{16}$$

In our model, the molecular vibrations are assumed to be half excited behind the main shock and not excited in front of the main shock [3]. Hence, the ratio of specific heats γ changes across the shock. In front of the main shock $\gamma_1 = 7/5$ and behind the main shock $\gamma_2 = 4/3$. For this case, the shock pressure ratio at the main shock is

$$\frac{p_2}{p_1} = \left(\frac{1}{1+\gamma_2}\right)\left\{\left(1+\gamma_1 M_{1N}^2\right) + \sqrt{\gamma_2^2+\gamma_1 M_{1N}^2\left[\gamma_1 M_{1N}^2 - 2\left(\frac{\gamma_2^2-\gamma_1}{\gamma_1-1}\right)\right]}\right\}, \tag{17}$$

which can be derived from the R-H conditions.

Since the free stream is uniform, the quantities in front of the main shock are

$$\begin{aligned} \frac{u_1}{V_\infty} &= 1, \\ \frac{v_1}{V_\infty} &= 0, \\ \frac{p_1}{\rho_\infty V_\infty^2} &= \frac{1}{\gamma_1 M_1^2}, \\ \frac{\rho_1}{\rho_\infty} &= 1. \end{aligned}$$

Using the space-marching technique to solve the problem means that when the solution at $\eta = \eta^*$ is known, we can use equations (12) and the boundary conditions (13-15) to get the solution at $\eta = \eta^* + \Delta\eta$ numerically. Then, the solution in the region $\eta_0^* < \eta \leq \eta_1^*$, $0 \leq \xi \leq 1$ can be obtained step by step.

In order to get numerical solutions, equations (12) have to be discretized. In many cases, the solution varies rapidly in some region in one direction, but is quite smooth elsewhere. For example,, the solution varies rapidly near the shock in the normal direction to the shock. If such a situation appears, in order to get accurate solution efficiently, a highly nonuniform mesh in that direction in the physical space is necessary. We propose to use a nonlinear smooth transformation function $G(\eta, \xi)$ to reach this purpose. Suppose the minimum mesh size in the physical space in the ξ-direction is very small and an explicit scheme is used. In this case, the mesh size in the η-direction must also be very small in order to guarantee the stability of computation. However, if an implicit scheme is used, a normal size in the η-direction can be adopted, which usually makes the computation more efficient. In addition, since we are dealing with the Euler equations and chemical equations fully coupled, there are possible numerical difficulties associated with the stiffness. To overcome these problems, the right-hand side should be dealt with implicitly. Keeping these facts in mind, we use a two-step second-order implicit finite difference scheme with implicit treatment of the right-hand side terms in our computation.

We shall use the following symbols in describing the finite difference methods for two dimensional problems:

$$\begin{aligned} \Delta \boldsymbol{U}_m &= \boldsymbol{U}_{m+\frac{1}{2}} - \boldsymbol{U}_{m-\frac{1}{2}}, \\ \mu f_m &= \frac{1}{2}\left(f_{m+\frac{1}{2}} + f_{m-\frac{1}{2}}\right), \end{aligned}$$

where $\boldsymbol{U}_m$, f_m denote $\boldsymbol{U}_m$, f at $\xi = m\Delta\xi$, $\Delta\xi$ being the mesh size in the ξ-direction.

We will discretize the equations (12) in two steps as follows [9]. At the first step, the scheme is

$$\mu\boldsymbol{A}^{*k}_{m+\frac{1}{2}}\mu\boldsymbol{U}^{k+\frac{1}{2}}_{m+\frac{1}{2}} + \frac{1}{2}\frac{\Delta\eta}{\Delta\xi}\mu\boldsymbol{B}^{*k}_{m+\frac{1}{2}}\Delta\boldsymbol{U}^{k+\frac{1}{2}}_{m+\frac{1}{2}} = \mu\boldsymbol{A}^{*k}_{m+\frac{1}{2}}\mu\boldsymbol{U}^{k}_{m+\frac{1}{2}} + \frac{1}{2}\Delta\eta\mu f^{k+\frac{1}{2}}_{m+\frac{1}{2}}, \tag{18}$$

which is a nonlinear equation with respect to $\boldsymbol{U}^{k+\frac{1}{2}}_m$. Here, $\boldsymbol{U}^k_m$ denotes $\boldsymbol{U}$ at $\xi = m\Delta\xi$ and $\eta = k\Delta\eta$, $\Delta\eta$ being the mesh size in the η-direction. In order to reduce the amount of computation, using the approximation

$$f^{k+\frac{1}{2}}_m \approx f^k_m + Df^k_m(\boldsymbol{U}^{k+\frac{1}{2}}_m - \boldsymbol{U}^k_m), \tag{19}$$

where Df is the gradient of f. We modify the scheme to

$$\begin{aligned}&\mu\boldsymbol{A}^{*k}_{m+\frac{1}{2}}\mu\boldsymbol{U}^{k+\frac{1}{2}}_{m+\frac{1}{2}} + \frac{1}{2}\frac{\Delta\eta}{\Delta\xi}\mu\boldsymbol{B}^{*k}_{m+\frac{1}{2}}\Delta\boldsymbol{U}^{k+\frac{1}{2}}_{m+\frac{1}{2}} - \frac{1}{2}\Delta\eta\mu\left[Df^k_{m+\frac{1}{2}}\boldsymbol{U}^{k+\frac{1}{2}}_{m+\frac{1}{2}}\right]\\ &= \mu\boldsymbol{A}^{*k}_{m+\frac{1}{2}}\mu\boldsymbol{U}^{k}_{m+\frac{1}{2}} + \frac{1}{2}\Delta\eta\mu f^k_{m+\frac{1}{2}} - \frac{1}{2}\Delta\eta\mu\left[Df^k_{m+\frac{1}{2}}\boldsymbol{U}^{k}_{m+\frac{1}{2}}\right],\end{aligned} \tag{20}$$

or when grouped in m,

$$\begin{aligned}&\frac{1}{2}\left(\mu\boldsymbol{A}^{*k}_{m+\frac{1}{2}} + \frac{\Delta\eta}{\Delta\xi}\mu\boldsymbol{B}^{*k}_{m+\frac{1}{2}} - \frac{1}{2}\Delta\eta Df^k_{m+1}\right)\boldsymbol{U}^{k+\frac{1}{2}}_{m+1}\\ &+\frac{1}{2}\left(\mu\boldsymbol{A}^{*k}_{m+\frac{1}{2}} - \frac{\Delta\eta}{\Delta\xi}\mu\boldsymbol{B}^{*k}_{m+\frac{1}{2}} - \frac{1}{2}\Delta\eta Df^k_m\right)\boldsymbol{U}^{k+\frac{1}{2}}_m\\ &= \mu\boldsymbol{A}^{*k}_{m+\frac{1}{2}}\mu\boldsymbol{U}^{k}_{m+\frac{1}{2}} + \frac{1}{2}\Delta\eta\mu f^k_{m+\frac{1}{2}} - \frac{1}{2}\Delta\eta\mu\left[Df^k_{m+\frac{1}{2}}\boldsymbol{U}^{k}_{m+\frac{1}{2}}\right].\end{aligned} \tag{21}$$

For the second step, the scheme is

$$\begin{aligned}&\mu\boldsymbol{A}^{*k+\frac{1}{2}}_{m+\frac{1}{2}}\mu\boldsymbol{U}^{k+1}_{m+\frac{1}{2}} + \frac{1}{2}\frac{\Delta\eta}{\Delta\xi}\mu\boldsymbol{B}^{*k+\frac{1}{2}}_{m+\frac{1}{2}}\Delta\boldsymbol{U}^{k+1}_{m+\frac{1}{2}}\\ &= \mu\boldsymbol{A}^{*k+\frac{1}{2}}_{m+\frac{1}{2}}\mu\boldsymbol{U}^{k}_{m+\frac{1}{2}} - \frac{1}{2}\frac{\Delta\eta}{\Delta\xi}\mu\boldsymbol{B}^{*k+\frac{1}{2}}_{m+\frac{1}{2}}\Delta\boldsymbol{U}^{k}_{m+\frac{1}{2}} + \frac{1}{2}\Delta\eta\left[\mu f^k_{m+\frac{1}{2}} + \mu f^{k+1}_{m+\frac{1}{2}}\right].\end{aligned} \tag{22}$$

Then using the approximation

$$f^{k+1}_m \approx f^k_m + Df^{k+\frac{1}{2}}_m(\boldsymbol{U}^{k+1}_m - \boldsymbol{U}^k_m) \tag{23}$$

at $m + \frac{1}{2}$, we obtain the scheme we will actually use in our computation

$$\begin{aligned}&\mu\boldsymbol{A}^{*k+\frac{1}{2}}_{m+\frac{1}{2}}\mu\boldsymbol{U}^{k+1}_{m+\frac{1}{2}} + \frac{1}{2}\frac{\Delta\eta}{\Delta\xi}\mu\boldsymbol{B}^{*k+\frac{1}{2}}_{m+\frac{1}{2}}\Delta\boldsymbol{U}^{k+1}_{m+\frac{1}{2}} - \frac{1}{2}\Delta\eta\mu\left[Df^{k+\frac{1}{2}}_{m+\frac{1}{2}}\boldsymbol{U}^{k+1}_{m+\frac{1}{2}}\right]\\ &= \mu\boldsymbol{A}^{*k+\frac{1}{2}}_{m+\frac{1}{2}}\mu\boldsymbol{U}^{k}_{m+\frac{1}{2}} - \frac{1}{2}\frac{\Delta\eta}{\Delta\xi}\mu\boldsymbol{B}^{*k+\frac{1}{2}}_{m+\frac{1}{2}}\Delta\boldsymbol{U}^{k}_{m+\frac{1}{2}}\\ &\quad+\Delta\eta\mu f^k_{m+\frac{1}{2}} - \frac{1}{2}\Delta\eta\mu\left[Df^{k+\frac{1}{2}}_{m+\frac{1}{2}}\boldsymbol{U}^{k}_{m+\frac{1}{2}}\right],\end{aligned} \tag{24}$$

or when grouped in m, the scheme becomes

$$\begin{aligned}
&\frac{1}{2}\left(\mu\boldsymbol{A}^{*k+\frac{1}{2}}_{m+\frac{1}{2}}+\frac{\Delta\eta}{\Delta\xi}\mu\boldsymbol{B}^{*k+\frac{1}{2}}_{m+\frac{1}{2}}-\frac{1}{2}\Delta\eta D f^{k+\frac{1}{2}}_{m+1}\right)\boldsymbol{U}^{k+1}_{m+1}\\
&+\frac{1}{2}\left(\mu\boldsymbol{A}^{*k+\frac{1}{2}}_{m+\frac{1}{2}}-\frac{\Delta\eta}{\Delta\xi}\mu\boldsymbol{B}^{*k+\frac{1}{2}}_{m+\frac{1}{2}}-\frac{1}{2}\Delta\eta D f^{k+\frac{1}{2}}_{m}\right)\boldsymbol{U}^{k+1}_{m} \qquad (25)\\
&\quad=\mu\boldsymbol{A}^{*k+\frac{1}{2}}_{m+\frac{1}{2}}\mu\boldsymbol{U}^{k}_{m+\frac{1}{2}}-\frac{1}{2}\frac{\Delta\eta}{\Delta\xi}\mu\boldsymbol{B}^{*k+\frac{1}{2}}_{m+\frac{1}{2}}\Delta\boldsymbol{U}^{k}_{m+\frac{1}{2}}\\
&\qquad+\Delta\eta\mu f^{k}_{m+\frac{1}{2}}-\frac{1}{2}\Delta\eta\mu\left[D f^{k+\frac{1}{2}}_{m+\frac{1}{2}}\boldsymbol{U}^{k}_{m+\frac{1}{2}}\right].
\end{aligned}$$

Our method is a shock-fitting method [6, 9]. The location of the shock, the function $r=c(\eta)$ has to be determined during the computation. For this purpose, we have the following second-order scheme

$$c^{k+\frac{1}{2}}=c^{k}+\frac{\Delta\eta}{2}c^{k}_{\eta}, \qquad (26)$$

and

$$c^{k+1}=c^{k}+\Delta\eta c^{k+\frac{1}{2}}_{\eta}. \qquad (27)$$

The concrete computational procedure is as follows. Suppose the solution is given at $\eta=\eta^*$, i.e., $\boldsymbol{U}$ at $\xi=0,\Delta\xi,2\Delta\xi,\cdots,M\Delta\xi$ and c, c_η are given, where $\Delta\xi=1/M$. Discretizing (12) by using scheme (21) at $\xi=(m+1/2)\Delta\xi$, $m=0,1,\cdots,M-1$, we obtain $6M$ equations, in which unknowns are $\boldsymbol{U}_0,\boldsymbol{U}_1,\cdots,\boldsymbol{U}_M$. Putting those equations and the boundary condition at the body (13) together, we have $6M+1$ equations in which there are $6(M+1)$ unknowns. Using elimination, we can obtain M relations of the form

$$\boldsymbol{U}_{m-1}=\boldsymbol{C}_m\boldsymbol{U}_m+\boldsymbol{D}_m,\quad m=M,M-1,\cdots,1. \qquad (28)$$

and a relation in which only $\boldsymbol{U}_M$ appears [9]. Solving this equation and the boundary conditions at the shock (14-15), we can determine $\boldsymbol{U}_M$ and c_η. Finally, using (28) and (26), we can get the rest part of the solution, i.e., $\boldsymbol{U}_{M-1},\boldsymbol{U}_{M-2},\cdots,\boldsymbol{U}_0$ and c at $\eta=\eta^*+\Delta\eta/2$. When the solutions at $\eta=\eta^*+\Delta\eta$ and $\eta=\eta^*+\Delta\eta/2$ are known, the solution at $\eta=\eta^*+\Delta\eta$ can be obtained by using the schemes (25), (27) and the boundary conditions (13-15) in a similar way.

Based on the method described here, a computer code has been written in Fortran. In the code, the mesh size in the η-direction is self-adjusted according to a given error level for an accurate and efficient computation.

4. Numerical Results

Figure 1 shows a qualitative picture of reacting flow in a neighborhood of the corner. The chemical reactions are frozen at the shock surface. Therefore, the concentrations of species are not changed across the shock. The high temperature immediately behind the shock causes significant reactions there. As the chemical relaxation occurs, the temperature drops and this in turn reduces the chemical reactions. Therefore, big rates of chemical reactions occur only at a small distance from the shock. The narrow strip B behind the shock in Figure 1 represents the chemical layer where chemical reactions are strong. Close to the corner, the chemical layer is not small compared to the shock layer. Therefore, it could be spread over many numbers of grids and we do not expect numerical difficulties associated with lack of resolutions. Far down stream, the chemical layer is a very small fraction of the shock layer because the physical thickness of the chemical layer remains almost unchanged while the shock layer becomes very

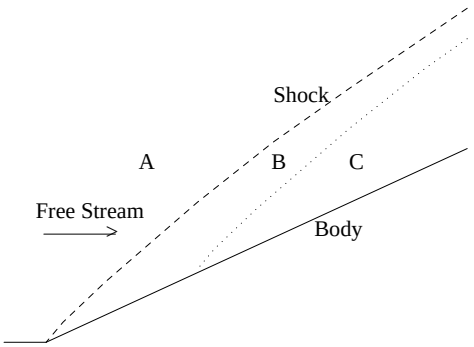

Figure 1. Flow about a concave corner

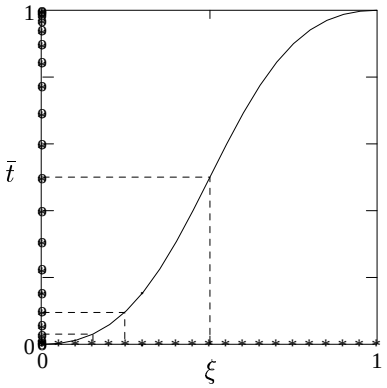

Figure 2. Coordinate transform

large. This nonequilibrium region causes numerical difficulties down stream because of lack of resolution in finite approximations near the shock if the mesh size is not small enough. Pandolfi *et al.* [4] found that when one grid was extended for an appreciable amount of the physical thickness of the chemical layer, the lack of accuracy behind the shock deteriorated the basic conservation properties in their computation.

To overcome those difficulties, we introduce such a smooth nonlinear monotone transformation function $r = G(\eta, \xi)$ that many computational grids are concentrated near the boundaries in the physical domain when a uniform mesh is used in the computational domain. For this purpose, we propose that $r = G(\eta, \xi)$ be implicitly defined by the following expression:

$$\xi = \frac{f^{-1}(t) - f^{-1}(\tau_1)}{f^{-1}(\tau_2) - f^{-1}(\tau_1)}, \tag{29}$$

where

$$\begin{aligned} f(t) &= \frac{2t}{t^2+1}, \\ t &= \bar{t}(\tau_2 - \tau_1) + \tau_1, \quad -1 < \tau_1 < 0 < \tau_2 < 1, \\ \bar{t} &= \frac{r - b(\eta)}{c(\eta) - b(\eta)}, \quad b(\eta) < r < c(\eta). \end{aligned} \tag{30}$$

The transformation depends on two parameters τ_1 and τ_2 and we used $\tau_1 = -0.999$, $\tau_2 = 0.9999$ for our computation about a concave corner to put many grid points near the body as well as near the shock. In this case the first few intervals behind the shock represent very small part of the shock layer. Thus, the chemical layer is spread over several intervals even at a large distance from the corner. Near the body the same technique is used to deal with the entropy layer. In Figure 2, the pattern of the arrangement of nodes in the r-direction is shown on the ordinate $\bar{t}$ if a uniform mesh size is used in ξ.

Far behind the chemical layer is the equilibrium region where all the reactions have gone to almost completion, which is the region C in Figure 1. In this region all the particles have almost reached their equilibrium states. The particles near the body and those far above have different equilibrium status because the former has crossed a stronger shock. This means that there is an entropy layer near the body. When we choose the function $G(\eta, \xi)$, this fact has been considered.

We have done some numerical experiments over a 30 degree wedge with free stream conditions as in Table 1. Our computation starts at the corner and the initial values are single-valued

Speed	$6.77\ Km/s$
Altitude	$65\ Km$
Pressure	$10.85\ N/m^2$
Density	$1.56 \times 10^{-4}\ Kg/m^3$
Temperature	$240.8\ K$
Mach Number	21.7

Table 1: Free Stream Conditions

and obtained by solving (14), (15) and (13). As mentioned in Section 3, the system of equations under consideration is integrated according to the space-marching technique along the coordinate η. We treat the shock with the shock-fitting technique [6, 9]. The jump conditions on shocks are the R-H conditions. If the slope of the shock is known, the quantities behind the shock can be determined by the R-H conditions. In practice, we guess the slope of the shock and use an iteration method to match the computed quantities with the equation obtained from finite difference method. Using our transformation and finite difference methods, we were able to continue the computation until a very large distance (over $3000\,m$) from the corner without encountering any numerical difficulties. Our computational results are shown in Figures 3 through 12.

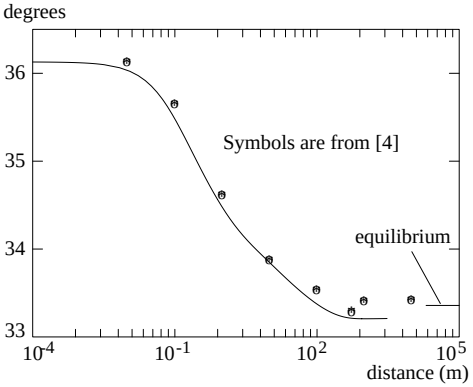

Figure 3. Shock angles

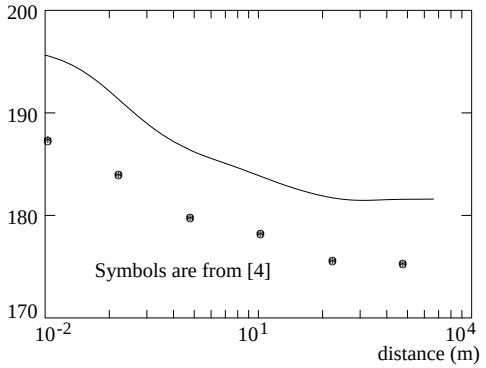

Figure 4. Pressure along the body

In Figure 3 our computational result of shock angle is given, which shows it reaches its limit at about $z = 1000\,m$. The initial shock angle is 36.13 degrees and the limit is 33.21 degrees. A slight undershoot reported in [4] is not noticeable in our result. In Figure 4, the pressure distribution along the body is given.

In Figures 5-12, variations of other quantities are given. There are actually two figures in each Figure. In the first one the ordinate is ξ and in the second one the ordinate is $\bar{t}$ and computed data are reported on the abscissa. The results are reported at $z = 0\,m$ (the initial value at the corner as solid line with $*$), $z = 0.054\,m$ (dashed line with x), $z = 0.340\,m$ (dotted line with o), $z = 4.349\,m$ (dot-and-dash with +), $z = 30.37\,m$ (solid line), $z = 99.1\,m$ (dashed line), $z = 669\,m$ (dotted line) and $z = 3000\,m$ (dot-and-dash). The enthalpy and temperature are real values. The concentrations of species O, N, NO are real values in unit $g\text{-}mole/g$. Other fluid dynamical quantities are relative values to the free stream. We did our computation with different mesh points in ξ-direction and the results are very close and, therefore, confirmed that

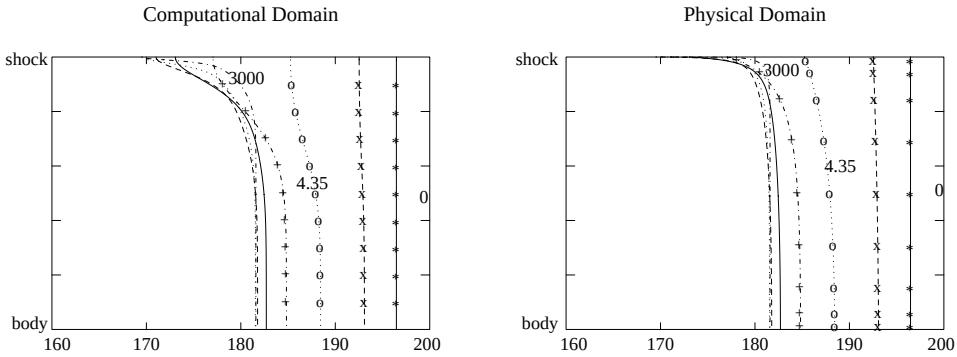

Figure 5. Pressure over shock layer

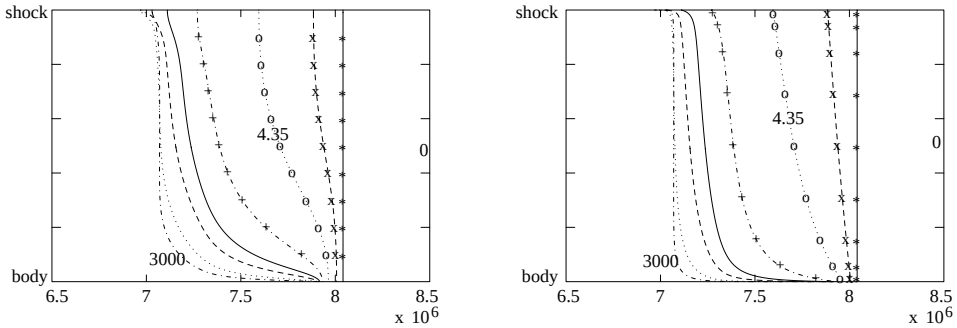

Figure 6. Enthalpy over shock layer

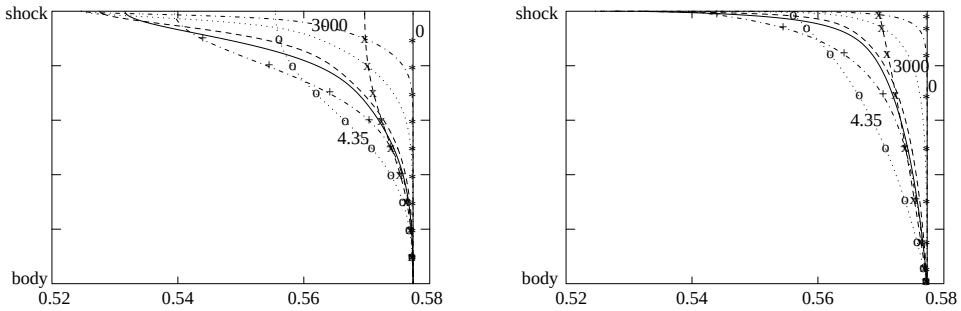

Figure 7. V/ U over shock layer

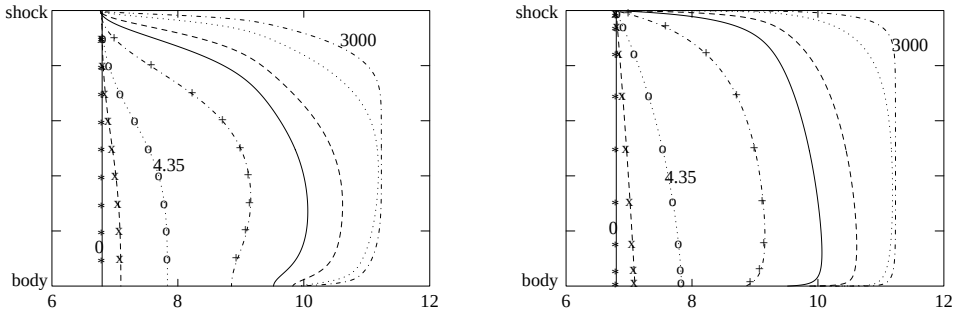

Figure 8. Density over shock layer

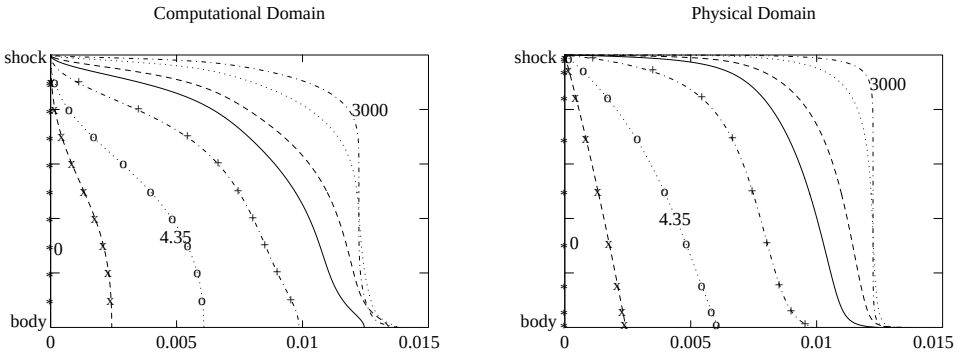

Figure 9. Concentration of O over shock layer

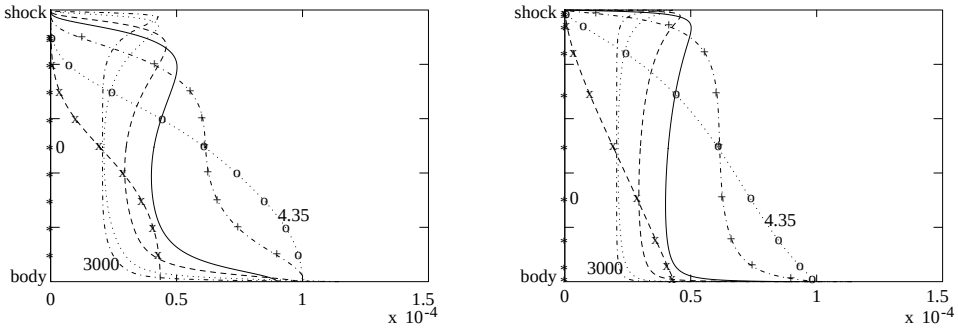

Figure 10. Concentration of N over shock layer

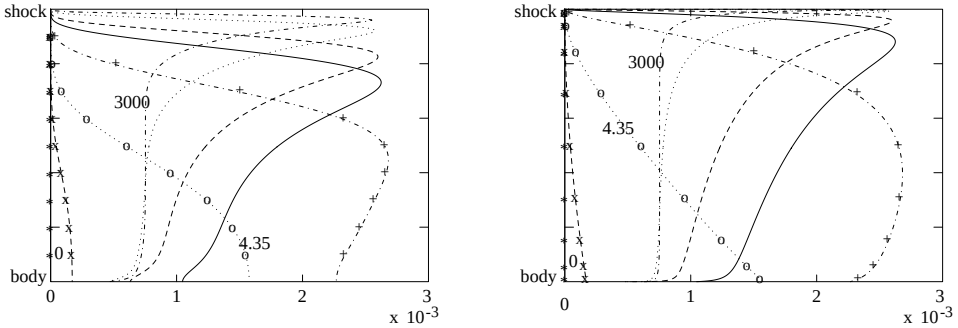

Figure 11. Concentration of NO over shock layer

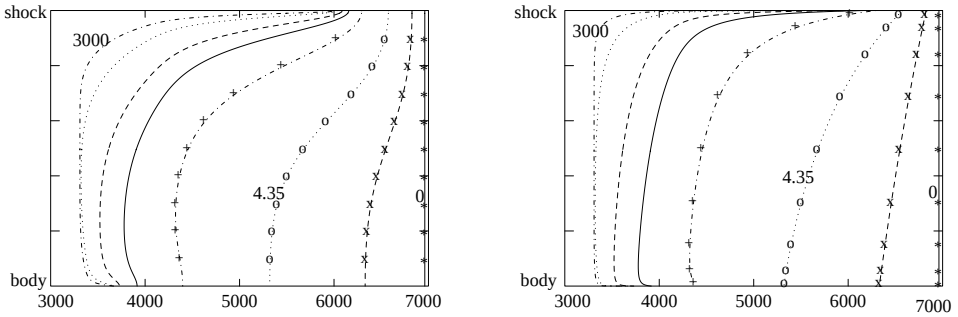

Figure 12. Temperature over shock layer

our results are accurate.

The concentrations of O, N and NO are monotonically decreasing in the ξ-direction for small z, which shows that the particles on the stream lines close to the body have spent a longer time in the chemical layer for dissociation. The concentration of NO is interesting. It already has reached its typical maximum near the body at $z = 4.349\,m$ and dissociation has already begun. Later the maximum peak moves toward the shock and it is very close to the shock at $z = 669\,m$. However, its maximum across the shock layer is almost constant. For O, N and NO, the concentrations near the body and near the shock are different from the values in the middle of the shock layer. Near the body, the flow consists of stream lines that cross the shock near the corner where the shock is stronger. Therefore, its equilibrium state is different from the flow far above the body. Near the shock, a chemical layer exists from the beginning to the far down stream. Also we can notice similar results for other properties. u, v, ρ and temperature converge to their uniform limit in the middle of the shock layer and have very different values in two small regions near the body and near the shock.

5. Conclusions

We have computed the hypersonic nonequilibrium flow over a concave corner. The model we have used is the well-known chemical model of 5-species and 18-reactions [7]. The vibrational excitation of biatomic molecules is assumed half-excited. That is, the vibrational mode is assumed to be excited always to such an extent that its energy content is $RT/2$. This half-excited model of Lighthill [3] is considered appropriate for our cases primarily because the vibrational energy is a small fraction of the static enthalpy and, hence, does not influence the flow quantities greatly [8].

We have gotten a solution of concave corner problem for a very long body. The longer the body is, the thinner the chemical layer is as compared with the shock layer and the more difficult the computation is. When the length of the body is fixed, the thickness of the chemical layer and the level of difficulty of the computation depend on the free stream conditions. Therefore, being able to do such a computation means that our method will work for the free stream conditions under which the computation for a body with a reasonable length, for example, $20\sim 30\,m$, is more difficult. The numerical technique includes a smooth transformation of domains, implicit finite difference schemes and implicit treatment of the right-hand side terms. By using the transformation of domains, we can put more grid points near boundaries where the flow quantities change very rapidly for accurate computations. In order to make the computation efficient, we adopt implicit difference schemes. The implicit treatment of the right-hand side terms is used to overcome difficulties arising from the stiffness. The exact location and strength of the shock are found by a shock fitting method [6, 9]. The shock angle decreases from the corner to the down stream and is stable at its limit after $1000\,m$. We were able to carry out our numerical experiments successfully. By comparing our result with others [4, 8] and comparing our results obtained by using different mesh points [5], we believe our results are accurate.

Acknowledgements. The first author wishes to express his sincere thanks to his advisor Dr. R. Cohen.

References

[1] Botta, N., Pandolfi, M. and Germano, M., Non-Equilibrium Reacting Hypersonic Flow About Blunt Bodies: Numerical Prediction, AIAA Paper 88-0514, 1988.

[2] Desideri, J.-A., Glinsky, N. and Hettena, E., Hypersonic Reactive Flow Computations, *Computers and Fluids*, **18**:2 (1990), 151-182.

[3] Lighthill, M. L., Dynamics of Dissociating Gas, Part I: Equilibrium Flow, *Journal of Fluid Mechanics*, **2**:1 (1957), 1-32.

[4] Pandolfi, M., Arina, R. and Botta, N., Nonequilibrium Hypersonic Flows over Corners, *AIAA Journal*, **29**:2 (1991), 235-241.

[5] Park, T., Computations of Nonequilibrium Hypersonic Inviscid Flow around Bodies, Ph.D. Dissertation, The University of North Carolina at Chapel Hill, 1994.

[6] Park, T., Zhu, Y.-l., Shock Interactions in Nonequilibrium Hypersonic Flow, *J. Comput. Math.*, **15**:3 (1997), 345-364.

[7] Rakich, J. V., Bailey, H. E., Park, C., Computation of Nonequilibrium Three-Dimensional Inviscid Flow over Blunt-Nosed Bodies Flying at Supersonic Speeds, AIAA Paper 75-835, 1975.

[8] Rakich, J. V., Bailey, H. E. and Park, C., Computation of Nonequilibrium, Supersonic Three-Dimensional Inviscid flow over Blunt-Nosed Bodies, *AIAA Journal*, **21**:6 (1983), 834-841.

[9] Zhu, Y.-l., Zhong, X.-c., Chen, B.-m. Zhang, Z.-m., Difference Methods for Initial-Boundary-Value Problems and Flow Around Bodies, Springer-Verlag, Heidelberg and Science Press, Beijing, 1988.